# Stability Analysis of Parallel Grid-Forming Inverters in Asymmetrical Conditions

Akhavan, Ali; Vasquez, Juan C.; Guerrero, Josep M.

*Published in:*
IEEE Journal of Emerging and Selected Topics in Industrial Electronics

*DOI (link to publication from Publisher):*
10.1109/JESTIE.2023.3337723



*Publication date:*
2024

*Document Version*
Accepted author manuscript, peer reviewed version

# Stability Analysis of Parallel Grid-Forming Inverters in Asymmetrical Conditions

Ali Akhavan, *Senior Member, IEEE*, Juan C. Vasquez, *Senior Member, IEEE*, and Josep M. Guerrero, *Fellow, IEEE*

***Abstract*—The stability of inverters can be greatly improved by designing them with a robust control system. However, even if the system remains stable under symmetrical conditions, the presence of asymmetrical load/grid impedance can still pose a threat to its stability. Under this circumstance, the coupling between the *αβ*- and *dq*-frames in the average model leads to the creation of a multi-input multi-output (MIMO) system. Consequently, simplifying the system into a single-input single-output (SISO) form is no longer feasible. This situation becomes even more complex when multiple inverters are connected in parallel, where the interaction among inverters complicates the modeling of the system. This paper presents a simple yet accurate approach to address these challenges. To this end, the models of the inverters in the frequency domain are lumped to investigate the stability of the entire system in light of the asymmetrical condition using the generalized Nyquist criterion.**

***Index Terms*—Asymmetrical conditions, parallel inverters, stability, grid-forming inverters.**

## I. Introduction

The stability of inverter-based systems is crucial in either voltage-controlled (grid-forming) or current-controlled (grid-following) modes for reliable operation. Different challenges such as the *LCL* filter resonance, the negative impact of the delay in digitally-controlled systems, and the interaction of inverters may threaten the stability of the system [1], [2]. Many works have been done to address these challenges. Different resonance damping methods [1], adding a positive phase to the system through high-and band-pass filters [3], and designing the control system based on passivity [4] are among the well-known approaches for addressing the mentioned challenges.

Even though all these works are admirable, however, they have considered a symmetrical condition. Assuming this condition simplifies the system analyses because one can analyze the system in a single-input single-output (SISO) form. Thus, the control system could be evaluated freely in either $\alpha/d$ or $\beta/q$ axis as they are mathematically equal. However, different factors especially in islanded systems such as asymmetrical loads make the system structure asymmetric. Research studies indicate that the stability of the system may be endangered by system asymmetry. The generalized Nyquist criterion (GNC) was employed in [5] to conduct the stability analysis of an inverter equipped with the *L* filter under asymmetrical grid impedance conditions. The investigation of inverter behavior under asymmetrical grid conditions was expanded by Wu *et al.* [6] through an analysis of a current-controlled inverter with an *LCL* filter. Their findings indicate that the presence of system asymmetry leads to coupling between the $\alpha$ and $\beta$ axes, making it impossible to simplify the system into a single-input single-output (SISO) form, due to its multi-input multi-output (MIMO) structure.

An analysis of the stability of parallel inverters is proposed in this paper to address this problem. For stability analysis of parallel inverters, the frequency model of each inverter is derived, then, an aggregated model is built. Afterward, the effect of the asymmetrical load on the system is elaborated. It is shown that by examining only two eigenvalues from the combined model, one can predict the stability of parallel inverters, making this method a promising approach for analyzing stability in large-scale systems.

This work was supported by the VILLUM FONDEN under the VILLUM Investigator Grant 25920, Center for Research on Microgrids (CROM).

The authors are with AAU Energy, Aalborg University, Aalborg, Denmark (e-mail: alak@energy.aau.dk; juq@energy.aau.dk; joz@energy.aau.dk).

## II. System Overview

Fig. 1 shows the typical configuration of a system with *n* parallel inverters, where $L_1$, $L_2$, and $C$ are the inverter- and grid-side inductors, and filter capacitor, respectively, where their associated impedances are as follows:

$$Z_{L1} = L_1 s,\ Z_{L2} = L_2 s,\ Z_C = \frac{1}{Cs} \tag{1}$$

Also, $Z_{Load,i}$ ($i$ = $a$, $b$, $c$) is the load impedance, which could have different values in each line. Fig. 1 shows inverters connected to a passive load, however, the analysis is applicable to both islanded and grid-connected modes since grid-forming inverters can operate in either mode.

### A. Control System

Fig. 2 illustrates the control block diagram of inverters for each phase. A dual-loop control system is employed to regulate the capacitor voltage, in which a proportional-resonant (PR) regulator for the voltage regulator and a proportional regulator for the current regulator are used, denoted as $G_v(s)$ and $k_{pi}$, respectively [7]. Active damping is implemented by using the proportional gain $k_{AD}$ for mitigation of the *LCL* filter resonance [7]. The model for the lumped sampling and PWM delays is represented by $G_d(s)$ as [1]

$$G_d(s) = e^{-1.5\,T_s s} \tag{2}$$

### B. Deriving the Frequency Model

By utilizing block diagram algebra and referring to Fig. 2, one can derive the capacitor voltage as shown below:

$$v_c(s) = G_{cl}(s)v_{ref}(s) - Z_o(s)i_o(s) \tag{3}$$

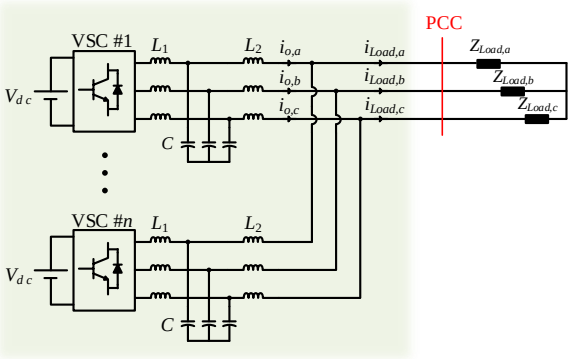


Fig. 1. The grid-forming system consisting of $n$ parallel inverters.

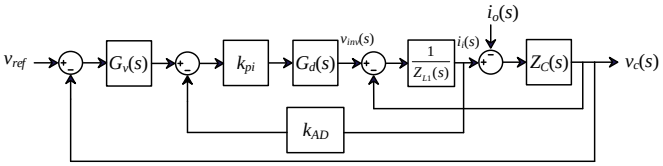

Fig. 2. The control block diagram of grid-forming inverters.

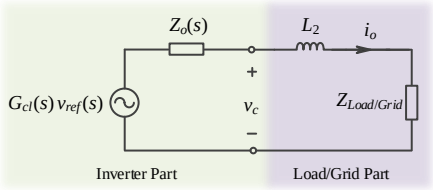


Fig. 3. The Thevenin equivalent model for grid-forming inverters.

where the transfer functions of the closed-loop system and the output impedance of the inverter are $G_{cl}(s)$ and $Z_o(s)$ as:

$$G_{cl}(s)=\frac{k_{pi}G_v(s)G_d(s)Z_C(s)}{Z_{L1}(s)+Z_C(s)+k_{pi}k_{AD}G_d(s)+k_{pi}G_v(s)G_d(s)Z_C(s)} \tag{4}$$

$$Z_o(s)=\frac{Z_{L1}(s)Z_C(s)+k_{pi}k_{AD}Z_C(s)G_d(s)}{Z_{L1}(s)+Z_C(s)+k_{pi}k_{AD}G_d(s)+k_{pi}G_v(s)G_d(s)Z_C(s)} \tag{5}$$

From Fig. 2, it can be found that the impedance $Z_{L2}$ can be considered as a part of the load/grid impedance. Regarding (3), the Thevenin equivalent circuit of the inverter in the frequency domain is derived as illustrated in Fig. 3. By substituting each inverter in Fig. 1 with its Thevenin equivalent, Fig. 4(a) could be achieved. Assuming similar inverters in the system, the aggregated model for $n$ parallel inverters could be derived as illustrated in Fig. 4(b).

## III. Stability Analysis

Regarding Fig. 4(b), the capacitor voltage of the aggregated model could be expressed as

$$\begin{bmatrix} v_{c,a}(s) \\ v_{c,b}(s) \\ v_{c,c}(s) \end{bmatrix} = \begin{bmatrix} G_{cl}(s) & & \\ & G_{cl}(s) & \\ & & G_{cl}(s) \end{bmatrix} \begin{bmatrix} v_{ref,a}(s) \\ v_{ref,b}(s) \\ v_{ref,c}(s) \end{bmatrix} - \begin{bmatrix} \frac{Z_o(s)}{n} & & \\ & \frac{Z_o(s)}{n} & \\ & & \frac{Z_o(s)}{n} \end{bmatrix} \begin{bmatrix} i_{load,a}(s) \\ i_{load,b}(s) \\ i_{load,c}(s) \end{bmatrix} \tag{6}$$

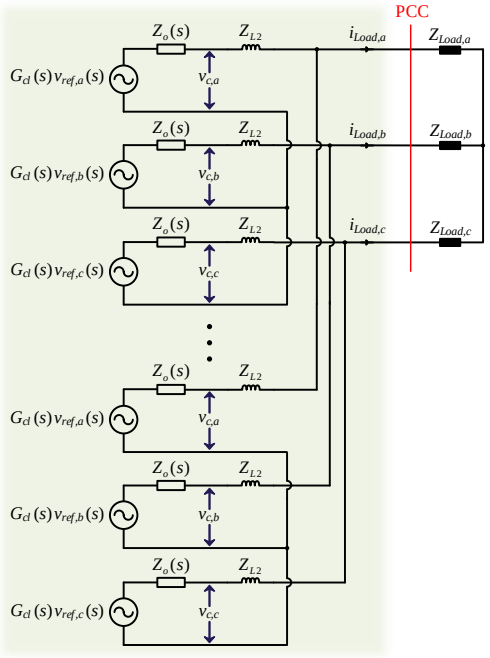


(a)

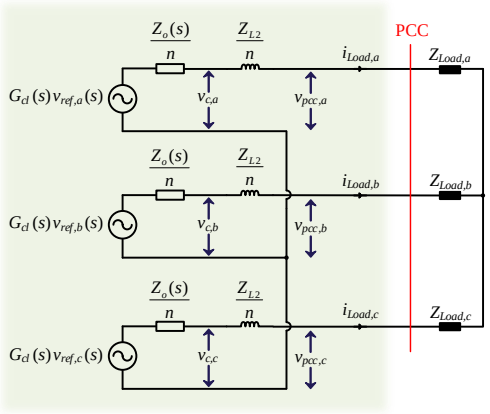


(b)

Fig. 4. The frequency model for $n$ parallel grid-forming inverters. (a) Actual model. (b) Aggregated model.

Also, the load current could be derived as follows:

$$\begin{bmatrix} i_{Load,a}(s) \\ i_{Load,b}(s) \\ i_{Load,c}(s) \end{bmatrix} = \begin{bmatrix} \left(\frac{Z_{L2}(s)}{n}+Z_{Load,a}\right)^{-1} & & \\ & \left(\frac{Z_{L2}(s)}{n}+Z_{Load,b}\right)^{-1} & \\ & & \left(\frac{Z_{L2}(s)}{n}+Z_{Load,c}\right)^{-1} \end{bmatrix} \begin{bmatrix} v_{c,a}(s) \\ v_{c,b}(s) \\ v_{c,c}(s) \end{bmatrix} \tag{7}$$

By combining (6) and (7), the capacitor voltage could be obtained as (8), as presented at the bottom of the next page. To transform the system into the $\alpha\beta$ frame, the Clarke matrix in (9) is multiplied by both sides of (8), which results in (10).

$$\boldsymbol{T}_{abc\to\alpha\beta}=\frac{2}{3}\begin{bmatrix}1 & -\frac{1}{2} & -\frac{1}{2}\\ 0 & \frac{\sqrt{3}}{2} & -\frac{\sqrt{3}}{2}\end{bmatrix} \tag{9}$$

$$\begin{bmatrix}v_{c,\alpha}(s)\\ v_{c,\beta}(s)\end{bmatrix}= \tag{10}$$

$$\left([I]_{2\times2}+\begin{bmatrix}\frac{Z_o(s)}{n} & \\ & \frac{Z_o(s)}{n}\end{bmatrix}\times\begin{bmatrix}Y_{Load,\alpha\alpha} & Y_{Load,\alpha\beta}\\ Y_{Load,\beta\alpha} & Y_{Load,\beta\beta}\end{bmatrix}\right)^{-1}\times\begin{bmatrix}G_{cl}(s) & \\ & G_{cl}(s)\end{bmatrix}\times\begin{bmatrix}v_{ref,\alpha}(s)\\ v_{ref,\beta}(s)\end{bmatrix}$$

where diagonal and off-diagonal elements of the load admittance matrix $Y_{Load}$ are presented in (11). As could be found from (10) and (11), a coupling exists between the $\alpha$ and $\beta$ axes, caused by the asymmetry of the load impedance.

$$\begin{aligned}
Y_{Load,\alpha\alpha}&=\frac{2}{3}\left(\frac{Z_{L2}(s)}{n}+Z_{Load,a}\right)^{-1}+\frac{1}{6}\left(\frac{Z_{L2}(s)}{n}+Z_{Load,b}\right)^{-1}+\frac{1}{6}\left(\frac{Z_{L2}(s)}{n}+Z_{Load,c}\right)^{-1}\\
Y_{Load,\alpha\beta}&=Y_{Load,\beta\alpha}=\frac{\sqrt{3}}{6}\left(\left(\frac{Z_{L2}(s)}{n}+Z_{Load,c}\right)^{-1}-\left(\frac{Z_{L2}(s)}{n}+Z_{Load,b}\right)^{-1}\right)\\
Y_{Load,\beta\beta}&=\frac{1}{2}\left(\frac{Z_{L2}(s)}{n}+Z_{Load,b}\right)^{-1}+\frac{1}{2}\left(\frac{Z_{L2}(s)}{n}+Z_{Load,c}\right)^{-1}.
\end{aligned} \tag{11}$$

In this condition, the system is MIMO, and by ignoring the asymmetrical condition of the system, stability analysis of the system might result in an inaccurate stability prediction.

Without considering the matrix nature of (10), one can represent it as follows:

$$v_c(s)=\frac{1}{1+\frac{Z_o(s)}{n}Y_{Load}(s)}G_{cl}(s)v_{ref}(s) \tag{12}$$

Supposing that the closed-loop control system (i.e., $G_{cl}(s)$) of each inverter is designed to be individually stable, to investigate the stability of the overall system, it is necessary to analyze the stability of $1/(1+Z_o(s)Y_{Load}(s)/n)$. It represents the closed-loop transfer function of a system, where $Z_o(s)Y_{Load}(s)/n$ is the characteristic equation. Thus, if the characteristic equation is stable, the whole system also will be stable. Referring to (10), and based on the above explanation, the characteristic equation is presented in (13).

$$G_{CH}(s)=\begin{bmatrix}\frac{Z_o(s)}{n} & \\ & \frac{Z_o(s)}{n}\end{bmatrix}\times\begin{bmatrix}Y_{Load,\alpha\alpha} & Y_{Load,\alpha\beta}\\ Y_{Load,\beta\alpha} & Y_{Load,\beta\beta}\end{bmatrix} \tag{13}$$

TABLE I
SYSTEM AND CONTROL PARAMETERS

| | |
|---|---|
| Inductor $L_1$ | 3 mH |
| Capacitor $C$ | 15 µF |
| Inductor $L_2$ | 3 mH |
| DC voltage, $V_{dc}$ | 150 V |
| Sampling frequency, $f_s$ | 10 kHz |
| Nominal voltage (RMS) | 50 V (Phase voltage) |
| Power frequency | 50 Hz |
| Load | $Z_{Load.a}$ = 10Ω resistive<br>$Z_{Load.b}$ = 40µF or 50mH-4Ω in series<br>$Z_{Load.c}$ = 15Ω resistive |
| Voltage controller (Proportional-resonant controller) | $G_{v,\alpha}(s) = G_{v,\beta}(s)$<br>$= k_p + k_r \times s / (s^2 + \omega_o^2)$<br>$k_p$ = 0.1, $k_r$ = 500 |
| Current controller | $k_{pi,\alpha} = k_{pi,\beta}$ = 2.5 |
| Active damping controller | $k_{AD,\alpha} = k_{AD,\beta}$ = 5 |

To evaluate the stability of $G_{CH}(s)$, the generalized Nyquist criterion is employed. First, the eigenvalues of $G_{CH}(s)$ should be derived from (14).

$$\det\left[\lambda I-G_{CH}(s)\right]=0 \tag{14}$$

The system eigenvalues can be expressed by solving (14) as follows:

$$\lambda_{1,2}(s)=\frac{Z_o(s)}{2n}\times\left(\left(Y_{g,\alpha\alpha}+Y_{g,\beta\beta}\right)\pm\sqrt{\left(Y_{g,\alpha\alpha}-Y_{g,\beta\beta}\right)^2+4Y_{g,\alpha\beta}Y_{g,\alpha\beta}}\right) \tag{15}$$

In accordance with GNC, if a system is stable, the Nyquist diagrams of its eigenvalues will not encircle (-1, 0), i.e., the critical point. As could be concluded, a simple analysis of two eigenvalues would suffice for the stability investigation of a system, even one with a large number of parallel inverters.

## IV. Analytical and Experimental Results

The stability of two parallel inverters is analyzed here.

### *A. Stability Analysis of Two Parallel Inverters*

Two parallel inverters are considered in this section, and they feed different types of loads in each phase. Table I lists the system and control parameters. The control parameters in both $\alpha$ and $\beta$ axes are tuned intentionally identically even though each axis sees a different load impedance, to show the consequence of ignoring the asymmetrical condition. Details on how to design the control system for grid-forming inverters can be found in [7] and [8].

$$\begin{bmatrix}v_{c,a}(s)\\ v_{c,b}(s)\\ v_{c,c}(s)\end{bmatrix}=\left([I]_{3\times3}+\begin{bmatrix}\frac{Z_o(s)}{n} & & \\ & \frac{Z_o(s)}{n} & \\ & & \frac{Z_o(s)}{n}\end{bmatrix}\times\underbrace{\begin{bmatrix}\left(\frac{Z_{L2}(s)}{n}+Z_{Load,a}\right)^{-1} & & \\ & \left(\frac{Z_{L2}(s)}{n}+Z_{Load,b}\right)^{-1} & \\ & & \left(\frac{Z_{L2}(s)}{n}+Z_{Load,c}\right)^{-1}\end{bmatrix}}_{Y_{Load}^{abc}}\right)^{-1}\times\begin{bmatrix}G_{cl}(s) & & \\ & G_{cl}(s) & \\ & & G_{cl}(s)\end{bmatrix}\times\begin{bmatrix}v_{ref,a}(s)\\ v_{ref,b}(s)\\ v_{ref,c}(s)\end{bmatrix} \tag{8}$$

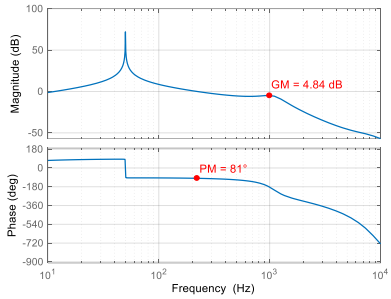


Fig. 5. The Bode diagram of the loop gain of the control system.

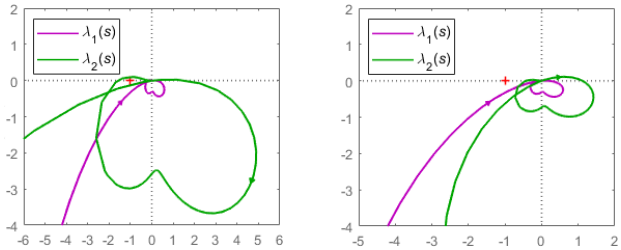


Fig. 6. The Nyquist diagrams of the eigenvalues $\lambda_1(s)$ and $\lambda_2(s)$. (a) $R_a$ = 10Ω, $C_b$ = 40μF, $R_c$ = 15Ω. (b) $R_a$ = 10Ω, $L_b$ = 50mH-$R_b$ = 4Ω, $R_c$ = 15Ω.

Fig. 5 displays the Bode diagram for the loop gain of the system illustrated in Fig. 2, with the control parameters from Table I, in order to demonstrate the stability of each inverter. The transfer function of the loop gain of the system, as shown in Fig. 2, is presented below:

$$T = \frac{G_v(s)k_{pi}G_d(s)Z_C(s)}{Z_{L1}(s)+Z_C(s)+k_{pi}k_{AD}G_d(s)} \tag{16}$$

Stability is evident in Fig. 5 because it has a positive phase- and gain margin. To simulate the system, a 10Ω resistor, a 40μF capacitor, and a 15Ω resistor are connected, respectively, to phases A, B, and C. The Nyquist diagrams are depicted in Fig. 6(a) for the eigenvalues $\lambda_1(s)$ and $\lambda_2(s)$. As could be observed, $\lambda_1(s)$ is stable because it does not encircle the critical point, but this is not the case for $\lambda_2(s)$. It reveals that the system is unstable, even though each inverter has a stable control system. Afterward, the capacitor of Phase B is replaced with a series *RL* load ($L$ = 50mH, $R$ = 4Ω). Fig. 6(b) displays the Nyquist diagrams for $\lambda_1(s)$ and $\lambda_2(s)$ in this scenario. It reveals that, unlike the previous case, both $\lambda_1(s)$ and $\lambda_2(s)$ are stable, which demonstrates that the entire system is stable under this asymmetrical load condition.

### *B. Experimental Results*

To examine the validity of the theoretical analysis, the experiments are carried out in the same condition that the theoretical analysis has been done. To this end, two parallel inverters are paralleled while they are connected to $R_a$ = 10Ω, $C_b$ = 40μF, and $R_c$ = 15Ω. Fig. 7 shows the load current in this case. Based on this figure, the system is unstable, confirming the theoretical analysis presented in Fig 6(a).

In the next step, the load in Phase B is replaced with a series *RL* load, where $L_b$ = 50mH, $R_b$ = 4Ω. The experimental outcome, displayed in Fig. 8, reveals that the system is stable under the new load condition, which validates Fig. 6(b).

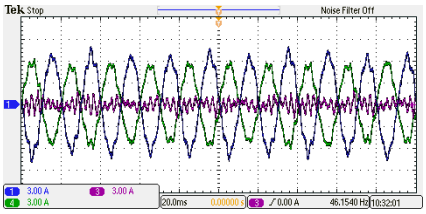


Fig. 7. The load current for the case of $R_a$ = 10Ω, $C_b$ = 40μF, $R_c$ = 15Ω.

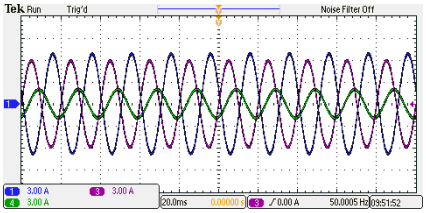


Fig. 8. The load current for the case of $R_a$ = 10Ω, $L_b$ = 50mH-$R_b$ = 4Ω, $R_c$ = 15Ω.

## V. Conclusion

This paper offers a simple and accurate approach for modeling parallel grid-forming inverters. The frequency model of each inverter is derived and replaced to obtain an aggregated model, simplifying stability analysis. This approach is highly advantageous for large-scale systems that comprise multiple parallel inverters, as the stability of the system can be assessed by examining only two eigenvalues.

## References


[1] X. Ruan, X. Wang, D. Pan, D. Yang, W. Li, and C. Bao, *Control Techniques for LCL-Type Grid-Connected Inverters*, Singapore, Singapore: Springer, 2018.

[2] J. L. Agorreta, M. Borrega, J. López, and L. Marroyo, "Modeling and control of *N*-paralleled grid-connected inverters with *LCL* filter coupled due to grid impedance in PV plants," *IEEE Trans. Power Electron.*, vol. 26, no. 3, pp. 770-785, Mar. 2011.

[3] A. Akhavan, H. R. Mohammadi, J. C. Vasquez, and J. M. Guerrero, "Passivity-based design of plug-and-play current-controlled grid-connected inverters," *IEEE Trans. Power Electron*, vol. 35, no. 2, pp. 2135-2150, Feb. 2020.

[4] L. Harnefors, X. Wang, A. Yepes, and F. Blaabjerg, "Passivity-based stability assessment of grid-connected VSCs—An overview," *IEEE J. Emerg. Sel. Topics Power Electron.*, vol. 4, no. 1, pp. 116–125, Mar. 2016.

[5] W. Liu, X. Wang, and F. Blaabjerg, "Modeling of unbalanced three-phase grid-connected converters with decoupled transfer functions," in *Proc. IEEE Int. Power Electron. Conf. (ECCE Asia)*, pp. 3164-3169, May 2018.

[6] W. Wu, J. Liu, Y. Li, and F. Blaabjerg, "Individual channel design-based precise analysis and design for three-phase grid-tied inverter with *LCL*-filter under unbalanced grid impedance," *IEEE Trans. Power Electron.*, vol. 35, no. 5, pp. 5381-5396, May 2020.

[7] A. Akhavan, S. Golestan, J. C. Vasquez, and J. M. Guerrero, "Passivity enhancement of voltage-controlled inverters in grid-connected microgrids considering negative aspects of control delay and grid impedance variations," *IEEE J. Emerg. Sel. Topics Power Electron.*, vol. 9, no. 6, pp. 6637-6649, Dec. 2021.

[8] Y. Geng, Y. Yun, R. Chen, K. Wang, H. Bai, and X. Wu, "Parameters design and optimization for *LC*-type off-grid inverters with inductor-current feedback active damping," *IEEE Trans. Power Electron.*, vol. 33, no. 1, pp. 703-715, Jan. 2018.